arXiv:1001.1292v3 [cond-mat.stat-mech] 17 Dec 2010

Confinement of Skyrmion states in noncentrosymmetric magnets

A. A. Leonov, A. N. Bogdanov, U. K. Rößler
IFW Dresden, Postfach 270116, D-01171 Dresden, Germany

(Dated: December 20, 2010)

Skyrmionic states in noncentrosymmetric magnets with Lifshitz invariants are investigated within the phenomenological Dzyaloshinskii model. The interaction between the chiral Skyrmions, being repulsive in a broad temperature range, changes into attraction at high temperatures. This leads to a remarkable *confinement* effect: near the ordering temperature Skyrmions exist only as bound states, and Skyrmion lattices are formed by an unusual instability-type nucleation transition. Numerical investigations on two-dimensional models demonstrate the confinement and the occurrence of different Skyrmion lattice precursor states near the ordering transition that can become thermodynamically stable by anisotropy or longitudinal softness in cubic helimagnets. We introduce a new fundamental parameter, *confinement temperature* T_p separating the peculiar region with "confined" chiral modulations from the main part of the phase diagram with regular helical and Skyrmion states.

PACS numbers: 75.10.-b 75.30.Kz 61.30.Mp 03.75.Lm

In certain noncentrosymmetric magnetic systems, the asymmetric Dzyaloshinskii-Moriya (DM) exchange results in chiral couplings that can stabilize long-period, non-collinear modulations of the magnetization with a *fixed* sense of rotation [1, 2]. These chiral couplings are phenomenologically described by Lifshitz invariants that destroy the homogeneity of ordered phases [1]. In highly symmetric systems with Lifshitz invariants multiple modulations occur as textures with localized twists in two or more spatial directions [3, 4]. In noncentrosymmetric magnetic systems with Lifshitz invariants these double-twist motifs exist as smooth (baby)-Skyrmions [5–7], static solitonic textures localized in two spatial directions, which can be extended into the third direction as Skyrmion strings or Hopfions. These magnetic Skyrmions are stabilized solely by the chiral DM couplings [6, 7], which prevent a spontaneous collapse into topological singularities. *Skyrmionic matter* is created by the condensation of these solitonic units, similar to vortex matter in type-II superconductors [5]. Just such chiral Skyrmions have been recently observed in thin layers of noncentrosymmetric ferromagnet (Fe,Co)Si [8]. Skyrmionic states stabilized by Lifshitz-type invariants may exist and form extended mesophases in various condensed matter systems, as chiral liquid crystals, ferroelectrics, multiferroics, and in confined achiral systems (e.g., thin magnetic layers) [4, 9–11].

Skyrmionic textures usually form through nucleation, following a classification introduced by DeGennes [12] for (continuous) transitions into incommensurate modulated phases. As demonstrated in Refs. [5, 6], for the low-temperature micromagnetic model of chiral magnets, at the transition from the field-driven Skyrmion lattices into the polarized homogeneous state the lattice period diverges and the Skyrmions are set free as localized excitations. As the Skyrmions retain their size and axisymmetric shape, there is a full spectrum of lattice modes up to the transition, in contrary to an instability type transition where the amplitude of one fundamental mode acts as small parameter of the transition [12].

Here, we show for the standard model of chiral isotropic ferromagnets [1, 7, 13] that Skyrmions are confined very close to the ordering temperature. In that part of the phase diagram, the creation of Skyrmions as stable units and their condensation into extended textures occurs simultaneously through a rare case of an instability-type nucleation transition [14], but the confined Skyrmions as discernible units may arrange in different mesophases. This is a consequence of the coupling between the magnitude and the angular part of the order parameter. Thus, near the ordering transitions, the local magnetization is not only multiply twisted but also longitudinally modulated. From numerical investigations on 2D models of isotropic chiral ferromagnets, a staggered half-Skyrmion square lattice at zero and low fields and a hexagonal Skyrmion lattice at larger fields are found in overlapping regions of the phase diagram near the transition temperature. Furthermore, the thermodynamic stability of Skyrmionic states can be favoured with respect to one-dimensional modulations by supplementing the model with cubic exchange anisotropy or in a modified model for metallic chiral magnets [7].

Within the standard phenomenological (Dzyaloshinskii) theory [1] the magnetic energy density of a noncentrosymmetric ferromagnet can be written in the dimensionless form [7, 13]

$$\Phi = (\mathbf{grad}\,\mathbf{m})^2 - w_D(\mathbf{m}) - h(\mathbf{n}\cdot\mathbf{m}) + am^2 + m^4. \quad (1)$$

Here, reduced values of the spatial variable $\mathbf{x} = \mathbf{r}/L_D$, the magnetization $\mathbf{m} = \mathbf{M}/M_0$, and the applied magnetic field $h\mathbf{n}$ ($h = |\mathbf{H}|/H_0$, $\mathbf{n}$ is a unity vector along $\mathbf{H}$), are expressed via the parameters of the energy density [13] $w(\mathbf{M}) = A(\mathbf{grad}\mathbf{M})^2 + Dw_D(\mathbf{M}) - \mathbf{H}\cdot\mathbf{M} + f(M)$ (where $f(M) = a_1M^2 + a_2M^4$, and $M = |\mathbf{M}|$): $L_D = A/D$, $H_0 = \kappa M_0$, $M_0 = (\kappa/a_2)^{1/2}$, $a = a_1/\kappa$, $\kappa = D^2/(A)$.

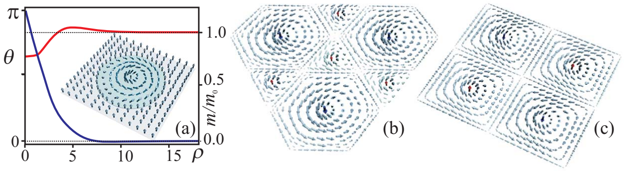

FIG. 1: (Color online) (a) Equilibrium solutions of localized Skyrmions, shown as cross section in the inset, display strong localization of $\theta(\rho)$ (blue) and weak variation of the magnetization modulus $m(\rho)$ (red) in a broad range of temperature and field (a, h). Exemplary profiles for $a = -0.25$, $h = 0.25$. (b) At lower fields, isolated Skyrmions condense into a dense-packed hexagonal lattice. (c) Near the ordering temperature $a_c = 0.25$ square lattice solutions with staggered *half-Skyrmion* cells arise.

DM energy w_D consists of Lifshitz invariants [1]

$$\mathcal{L}_{ij}^{(k)} = m_i(\partial m_j/\partial x_k) - m_j(\partial m_i/\partial x_k). \tag{2}$$

For noncentrosymmetric uniaxial ferromagnets DM functionals w_D are listed in [5]. In particular, for isotropic and cubic helimagnets $w_D(\mathbf{m}) = \mathcal{L}_{xz}^{(y)} + \mathcal{L}_{zy}^{(x)} + \mathcal{L}_{xy}^{(z)} = \mathbf{m}\cdot\mathrm{rot}\,\mathbf{m}$ [13] (for details see appendix). Functional (1) includes only the basic (*isotropic*) interactions essential to stabilize chiral modulations. This depends on three internal variables (components of the magnetization vector $\mathbf{m}$) and two control parameters, the reduced magnetic field amplutude h and the "effective" temperature $a(T)$. In chiral magnetism models (1) play a fundamental role and are similar to the Frank energy in liquid crystals and Landau-Ginzburg functional in superconductivity. We consider 2D chiral modulations homogeneous along the applied field $\mathbf{h}||z$ and modulated in the plane perpendicular $\mathbf{h}$.

Isolated and embedded Skyrmions. The equations minimizing functional (1) include solutions for axisymmetric localized states (*isolated Skyrmions*), $\psi = \psi(\phi)$, and $\theta(\rho)$, $m(\rho)$ where we use spherical coordinates for the magnetization (m, θ, ψ) and cylindrical coordinates for the spatial variables (ρ, ϕ, z). The solutions $\psi(\phi)$ for all noncentrosymmetric classes have been derived in [5]. For cubic helimagnets and uniaxial systems with $n22$ symmetry, $\psi = \phi - \pi/2$ (Fig. 1 a). Profiles $\theta(\rho)$ and $m(\rho)$ of isolated Skyrmions are derived from numerical solutions of the Euler equations, as given in Ref. 7 and common for all noncentrosymmetric classes with Lifshitz invariants, with the boundary conditions $\theta(0) = \pi$, $dm/d\rho(0) = 0$, $\theta(\infty) = 0$, $m(\infty) = m_0$ (m_0 is the magnetization in the saturated state). For extended textures of two-dimensional models, the functional has been investigated by numerical energy minimization using finite-difference discretization on rectangular grids with adjustable grid spacings [7].

Isolated Skyrmions (Fig. 1 (a)) exist only below a critical line h_0 and condense into a hexagonal lattice (Fig. 2) below a field h_c, which marks the transition between the Skyrmion lattice (SL) and the homogeneous paramagnetic state (see Fig. 2 (a), (b)). Near the ordering temperature a square *half-Skyrmion* lattice (Fig. 1 (c)) has lower energy than the hexagonal lattice. Half-SLs consist of cells with up and down magnetization in the center and in-plane magnetization along the cell boundaries. Such cells have a topological charge 1/2. In the hexagonal SLs the magnetization at the boundaries (center) is (anti)parallel to the applied field. The cells bear unit topological charges.

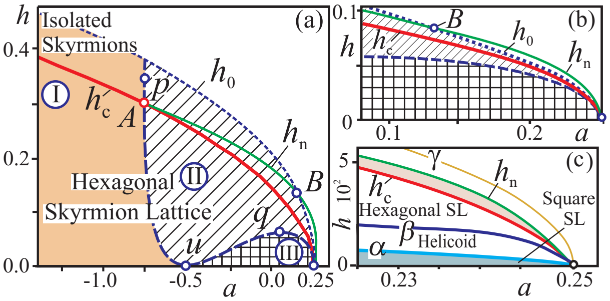

FIG. 2: (Color online) Field h vs. temperature a phase diagram. (a) Areas with *repulsive* (I) (shaded), *attractive* (II) Skyrmions (hatched), and strictly *confined* pocket (III) (cross-hatched) are separated by $h^\star$ (dashed line), Eq. (3). Isolated Skyrmions collapse at critical line h_0. Above this line no static Skyrmions exist. Below line h_c Skyrmions condense into a hexagonal lattice In region (II), the hexagonal Skyrmion lattice (SL) exists as metastable state up to the nucleation field h_n. For temperatures between points A and B, $h_n < h_0$, for larger temperatures $a_B < a < a_c = 0.25$ the isolated Skyrmions disappear at lower fields than the dense SL, $h_0 > h_n$. For clarity, line h_n is only schematically given in panel (a), numerically exact data are shown in panel (b). Detail of the phase diagram (c) near the ordering temperature shows the existence regions for different modulated states. Lines for first order transitions: α square half-SL ↔ hexagonal SL, β helicoid ↔ hexagonal SL. Line γ marks the continuous transition from the conical equilibrium phase in isotropic systems to the paramagnetic phase.

Confinement. By solving the linearized Euler equations for the asymptotics of isolated Skyrmions $\Delta m = (m - m_0)$, $\theta \propto \exp(-\kappa\rho)$ ($\rho \gg 1$) one finds three distinct regions in the magnetic phase diagram with different character of Skyrmion-Skyrmion interactions (Fig. 2 (a)): *repulsive* interactions in a broad temperature range (area (I)) are changed to *attractive* interaction at higher temperatures (area (II)). Finally in area (III) near the ordering temperature $a_c = 0.25$ strictly confined Skyrmions exist. These regions are separated by the line

$$h^\star = \sqrt{2 \pm P(a)}(a + 1 \pm P(a)/2), \; P(a) = \sqrt{3 + 4a} \tag{3}$$

with turning points p $(-0.75, \sqrt{2}/4)$, q $(0.06, 0.032\sqrt{5})$, and u (-0.5, 0) (dashed line in Fig. 2 (a)). In the major part of the phase diagram, the evolution of SLs under a

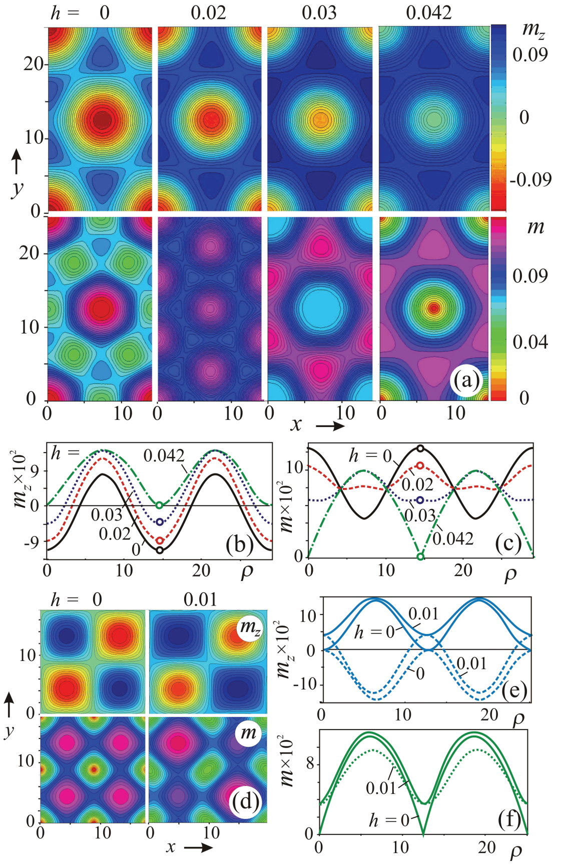

FIG. 3: (Color online) Numerically exact solutions for hexagonal (a)–(c) and square (d)–(f) Skyrmion lattices within the *confinement* pocket. Contour plots of $M_z(x, y)$ and $M(x, y)$ (a),(d) and their diagonal cross-sections (b),(e), (c),(f) are derived by minimization of Φ (1) with $a = 0.23$ and different values of the applied field. Solid (dashed) lines in panels (e), (f) indicate profiles for cells with (anti)parallel magnetization in the center.

magnetic field closely agrees with the behavior studied earlier for the low-temperature limit [5, 6] and the transition mechanism at the high-field limit is of the nucleation type with isolated Skyrmion excitations appearing below the instability line h_0. The temperature of the turning point p ($a_p = -0.75$), a *confinement* temperature T_c determines the frontier between low- ($T < T_p$) and high-temperature ($T_p < a < T_c$) chiral modulations. Usually $\Delta T = T_c - T_p \ll T_c$ and high-temperature modulations are restricted by a narrow vicinity of the Neel temperature. According to calculations in [7] for MnSi high-temperature Skyrmions exist in temperature interval $\Delta T = T_c - T_p = 2$ K below the Curie temperature T_c.

Evolution of confined Skyrmions. In the vicinity of the ordering temperature the Skyrmion lattices exist within the confinement pocket (III). In this region Skyrmion states drastically differ from those in the main part of the phase diagram. Due to the "softness" of the magnetization modulus the field-driven transformation of the Skyrmion lattices evolves by distortions of the modulus profiles $m(\rho)$ both in the hexagonal and square Skyrmion lattices while the equilibrium periods of the lattices do not change strongly with increasing applied field (Fig. 3). Despite the strong transformation of their internal structures the Skyrmion lattices preserve *axisymmetric* distribution of the magnetization near the centers of the Skyrmion lattice cells (Fig. 3). This remarkable property reflects the basic physical mechanism underlying the formation of Skyrmion lattices. The local energetic advantage of Skyrmion lattices over helicoids is due to a larger energy reduction in the "double-twisted" Skyrmion cell core compared to "single-twisted" helical states [4, 7]. This explains the unusual axial symmetry of the cell cores and their stability. An increasing magnetic field gradually suppresses the antiparallel magnetization in the cell core reducing the energetic advantage of the "double-twist" and increases the overall energy of the condensed Skyrmion lattice. At critical field h_c a first-order transition occurs into the polarized paramagnetic state. In the interval $h_c < h < h_n$ the hexagonal Skyrmion lattice exists as a metastable state. At the lability field h_n the magnetization modulus in the cell center becomes zero (see magnetization profile for $h = 0.042$ in Fig. 3 (c)). At this field, the "double-twist" region is suppressed, and the lattice loses its stability.

At zero field with increasing temperature a the magnetization modulus m in hexagonal and square lattices gradually decreases to zero at the ordering temperature. This is the instability-type nucleation transition into the paramagnetic phase : the order parameter m becomes zero at the transition point (as in the instability mode), however, the lattices retain their symmetry and the arrangement of axisymmetric Skyrmions up to the critical point. In finite fields in the region (II) the attractive Skyrmion-Skyrmion interaction means that multi-Skyrmions can always form bound states. Near a_c such clusters of Skyrmions are more stable than the isolated Skyrmions. This is seen in Fig. 2 (a),(b). For temperatures above point B, $a_B < a < a_c$, the metastable SL as the densest infinite cluster is more stable than isolated Skyrmions. Thus, in region (II) of the phase diagram, there is clustering and, for higher temperatures, confinement of isolated Skyrmion excitations.

The predicted Skyrmionic textures and the precursor phenomena associated with the confinement of Skyrmions near the ordering transition are observable in magnetic materials with appropriate symmetry. In a large group of *uniaxial noncentrosymmetric magnets* the DM energy is described by gradients only along directions perpendicular to the axis (e.g. multiferroic $BiFeO_3$, space group $R3c$ and antiferromagnetic $Ba_2CuGe_2O_7$, space group $P\bar{4}2_1m$ [2, 15]). In such magnets one-dimensional modulations with the propagation vector in the basal plane (*helicoids*) exist in broad ranges of the magnetic

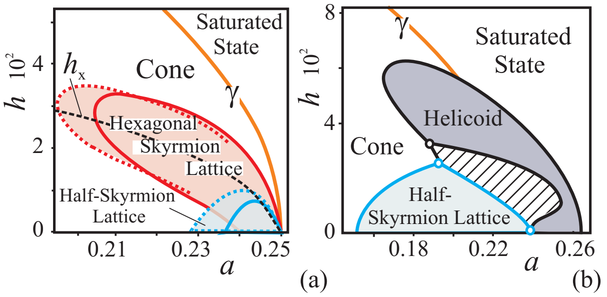

FIG. 4: (Color online) Magnetic phase diagrams of cubic helimagnets with exchange anisotropy $b = -0.05$ and the applied field along (111) (solid) and (001) (dashed) axes (a) contains regions with thermodynamically stable hexagonal SLs and half-SLs. Magnetic phase diagram of the modified isotropic model with $\eta = 0.8$ (b) has extended domains with thermodynamically stable helicoid, half-SLs and hexagonal SLs with the magnetization along the cell axes parallel to the magnetic field (hatched area).

fields [1, 16]. In the confinement pocket of the phase diagram (III) the helicoids also exist only as bound states [16]. They have the lowest energy at lower fields, and the hexagonal SL corresponds to the global energy minimum at higher fields (Fig. 2 (c)).

Cubic helimagnets. In other groups of chiral magnets the DM energy includes contributions with gradients along all three spatial directions. This stabilizes chiral modulations with propagation along the direction of an applied field as *cone* phases [13]. For the isotropic model $\Phi(\mathbf{m})$ (1) the cone phase solution with the fixed magnetization modulus and rotation of $\mathbf{m}$ around the applied magnetic field: $\psi = z$, $\cos(\theta) = h/m$, $m = |a - 1/2|/2$, is the global energy minimum in the whole region where modulated states exist. For cubic helimagnets, the energy density (1) has to be supplemented by anisotropic contributions, $\Phi_a = b \sum_i (\partial m_i/\partial x_i)^2 + k \sum_i m_i^4$, where b and k are reduced values of exchange and cubic anisotropies [13]. These anisotropic interactions impair the ideal harmonic twisting of the cone phase and lead to the thermodynamic stability of Skyrmion states, as shown in the equilibrium phase diagram Fig. 4 (a). The difference between the energy of the hexagonal Skyrmion lattice W_{sk} and of the cone phase W_{cone} calculated for the isotropic model, $\Delta W_{min} = W_{sk} - W_{cone}$, has minima along a curve $h_{\mathrm{x}}(a)$ which reaches the critical point $h_{\mathrm{x}}(a_c) = 0$ as $\Delta W_{min} = 0.0784(0.25 - a))$. Weak exchange anisotropy of a cubic helimagnet, therefore, creates a pocket around a_c, where the hexagonal Skyrmion lattice becomes the global energy minimum in a field (Fig. 4 (a)). This case is realized in cubic helimagnets with negative exchange anisotropy ($b < 0$) as in MnSi [13]. This anisotropy effect provides a basic mechanism, by which a Skyrmionic texture is stabilized in applied fields, as observed experimentally as so-called "A-phase" in MnSi [17–19]. The exchange anisotropy $b < 0$ also leads to the thermodynamic stability of half-SLs (Fig. 4 (a)). The stabilization of such textures may be responsible for anomalous precursor effects in cubic helimagnets in zero field [7, 20, 21].

Chiral modulations in non-Heisenberg models. A generalization of isotropic chiral magnets proposed in [7] replaces the usual Heisenberg-like exchange model by a non-linear sigma-model coupled to a modulus field with different stiffnesses. This yields a generalized gradient energy for a chiral isotropic system with a vector order parameter, which is equivalent to the phenomenological theory in the director formalism [4, 7] $\sum_{i,j} (\partial_i m_j)^2 \rightarrow \sum_{i,j} (\partial_i m_j)^2 + (1 - \eta) \sum_{i,j} (\partial_i m)^2 = m^2 \sum_{i,j} (\partial_i n_j)^2 + \eta \sum_i (\partial_i m)^2$. Parameter η equals unity for a "Heisenberg" model, in chiral nematics $\eta = 1/3$ [4]. Confined chiral modulations are very sensitive to values of $\eta < 1$. The magnetic phase diagram calculated for $\eta = 0.8$ includes pockets with square half-SLs, hexagonal SLs with the magnetization in the center of the cells parallel to the applied field, and helicoids with propagation transverse to the applied field (Fig. 4 b).

The confinement effects on chiral Skyrmions strongly changes the picture of the formation and evolution of chiral modulated textures and shed new light on the problem of precursor states observed as blue phases in chiral nematics [4] and in chiral magnets [7, 17–21]. The results show that confinement / deconfinement transitions of localized string-like solitons can be realized in these condensed matter systems. They provide counterparts of formation mechanisms for extended microscopic matter from topological solitons, as devised originally in the Skyrme model [22].

Acknowledgment. We thank K. v. Bergmann, G. Bihlmayer, S. Blügel, H. Eschrig, S.V. Grigoriev, J.-H. Han, S. Heinze, R. Mössner, C. Pappas, W. Selke, H. Wilhelm, and M. Zhitomirsky for discussions. Support by DFG project RO 2238/9-1 is gratefully acknowledged.

APPENDIX:DZYALOSHINSKII THEORY OF CHIRAL HELIMAGNETISM

The appendix includes technical comments on the mathematical structure of the interaction functional (1), on the mathematical relation between this model and those for different classes of noncentrosymmetric magnetic systems and chiral liquid crystals. The equations for isolated and bound Skyrmions are provided along with a short information on the numerical methods to solve these problems.

1. Basic model.

In noncentrosymmetric ferromagnets chiral asymmetry of exchange coupling related to the quantum-mechanical

Dzyaloshinskii-Moriya interactions [23] induces long-period modulations of the magnetization vector $\mathbf{M}$ with a fixed rotation sense [1]. The equilibrium chiral modulations are derived by minimization of the magnetic energy which can be written in the following general form [1]

$$W = A\sum_{i,j}(\partial M_j/\partial x_i)^2 - \mathbf{M}\cdot\mathbf{H} + W_0(\mathbf{M}) + W_D(\mathbf{M}) \quad (4)$$

where A is the exchange stiffness constant, $\mathbf{H}$ is an applied magnetic field, W_0 collects short-range magnetic interactions independent on spatial derivatives of the magnetization, and Dzyaloshinsky-Moriya energy W_D is composed of antisymmetric terms linear with respect to first spatial derivatives of the magnetization vector $\mathbf{M}(\mathbf{r})$

$$\mathcal{L}_{ij}^{(k)} = M_i\,(\partial M_j/\partial x_k) - M_i\,(\partial M_j/\partial x_k)\,.$$

Functional forms of W_D energy contributions are determined by crystallographic symmetry of a noncentrosymmetric magnetic crystal [1, 5, 13]. Particularly, for important cases of noncentrosymmetric ferromagnets belonging to cubic (23, 432) and uniaxial crystallographic classes ($n$mm, $\bar{4}$2m) the DM energy contributions have the following form [1, 5, 13]

$$\begin{aligned} W_D &= D\,(\mathcal{L}_{yx}^{(z)} + \mathcal{L}_{xz}^{(y)} + \mathcal{L}_{zy}^{(x)}) = D\,\mathbf{M}\cdot\mathrm{rot}\mathbf{M} \\ &\qquad\qquad\qquad\qquad\quad \text{for } (23), (432); \\ W_D &= D\,(\mathcal{L}_{xz}^{(x)} + \mathcal{L}_{yz}^{(y)}) \quad \text{for } (nmm); \\ W_D &= D\,(\mathcal{L}_{xz}^{(y)} + \mathcal{L}_{yz}^{(x)}) \quad \text{for } (\bar{4}2m) \end{aligned} \quad (5)$$

where $n = 3, 4, 6$ and D is a Dzyaloshinskii constant. For other noncentrosymmetric classes this W_D energy includes two or more Dzyaloshinskii constants [5].

Near the ordering temperatures the magnetization amplitude varies under the influence of the applied field and temperature. Commonly this process is described by including into the magnetic energy an additional term [13]

$$W \to W + a_1 M^2 + a_2 M^4,\ a_1 = J(T - T_c),\ a_2 > 0 \quad (6)$$

This model is fundamental to the systematic phenomenological description of magnetic states in noncentrosymmetric magnetic systems [1]. Interaction functional (4) plays in chiral magnetism a similar role as the *Frank energy* in liquid crystals [24] or *Ginzburg-Landau* functional in physics of superconductivity [25]. Its form is dictated by the natural extension of Landau's approach to ordering transtions for modulated systems which break the third Lifshitz condition, as pioneered by Dzyaloshinskii in particular in magnetism [26]. As a result, this type of theory constitutes the canonical form of statistical field theories for condensed matter systems, where particular couplings and symmetry enable Lifshitz invariants to induce modulated phases. Extensions including higher-order secondary effects in magnetism (like anisotropies or dipolar interactions) are widely used to describe evolution of modulated states in many chiral magnets [2, 6, 7, 27], including metamagnetic transitions in cubic helimagnets induced by high pressure [13, 28, 29].

By rescaling the spatial variable in (1),(6) $\mathbf{x} = \mathbf{r}/L_D$, the magnetic field $\mathbf{h} = \mathbf{H}/H_0$, the magnetization $\mathbf{m} = \mathbf{M}/M_0$

$$\begin{aligned} &L_D = A/D, \quad H_0 = \kappa M_0,\ M_0 = (\kappa/a_2)^{1/2}, \\ &\kappa = D^2/(2A),\ a = a_1/\kappa = J(T - T_c)/\kappa. \end{aligned} \quad (7)$$

energy W (6) can be written in the following reduced form (Eq. (1))

$$\Phi = (\mathbf{grad\,m})^2 - w_D(\mathbf{m}) - h(\mathbf{n}\cdot\mathbf{m}) + am^2 + m^4, \quad (8)$$

where $h = |\mathbf{h}|$ and $\mathbf{n}$ is a unity vector along the applied magnetic field. Functional (8) includes three internal variables (components of the magnetization vector $\mathbf{m}$) and two control parameters, the reduced magnetic field amplutude h and the "effective" temperature $a(T)$ (7). By direct minimization of Eq. (8) we have derived one-dimensional (kinks, helicoids, conical helices or spirals) and two-dimensional solutions (isolated and bound Skyrmions) for arbitrary values of the control parameters. These results are collected in the phase diagram of solutions (Fig. 2).

Energy (8) includes only basic interactions *essensial* to stabilize Skyrmionic and helical phases. Solutions for chiral modulated phases and their most general features attributed to all chiral ferromagnets are determined by interactions functional (8). Generically, there are only small energy differences between these different modulated states. On the other hand, weaker energy contributions (as magnetic anisotropy, stray-fields, magneto-elastic couplings) impose distortions on solutions of model (8) which reflect crystallographic symmetry and values of magnetic interactions in individual chiral magnets. These weaker interactions determine the stability limits of the different modulated states (Fig. 4). The fact that thermodynamical stability of individual phases and conditions of phase transfomations between them are determined by magnetocrystalline anisotropy and other relativistic or weaker interactions means that (i) the basic theory only determines a set of different and unusual modulated phases, while (ii) the transitions between these modulated states, and their evolution in magnetization processes depends on symmetry and details of magnetic secondary effects in chiral magnets, in particular the strengths of relativistic magnetic interactions. Thus functional (8) is the *generic* model for a manifold of interaction functionals describing different groups of noncentrosymmetric magnetic crystals, because it allows to identify the basic modulated structures that may be found in them.

2. Equations for isolated and bound Skyrmions

The Euler equations for functional (8) have solutions for axisymmetric isolated structures of type $\psi = \psi(\phi)$, $\theta(\rho)$, $m(\rho)$ (we introduce here spherical coordinates for the magnetization (m, θ, ψ) and cylindrical coordinates for the spatial variables (ρ, ϕ, z)) [7]. Solutions $\psi = \psi(\phi)$ are known for all uniaxial and cubic noncentrosymmetric ferromagnets [5]. Particularly, $\psi = \phi - \pi/2$ for cubic helimagnets, $\psi = \phi$ and $\psi = -\phi - \pi/2$ for uniaxial ferromagnets with (nmm) and $\bar{4}2m$ symmetry, correspondingly. After substitution of solutions $\psi = \psi(\phi)$ into (8) and integration with respect to ϕ the total energy E of a Skyrmion (per unit length along z) is $E = 2\pi \int_0^\infty \Phi(m, \theta)\rho d\rho$ with energy density

$$\Phi = m_\rho^2 + m^2 \left[\theta_\rho^2 + \frac{\sin^2\theta}{\rho^2} - \theta_\rho - \frac{\sin\theta\cos\theta}{\rho}\right] + am^2 + \\ +m^4 - hm\cos\theta \qquad (9)$$

where a common convention $\partial f/\partial x \equiv f_x$ is applied. The Euler equations for the functional (9)

$$m\left[\theta_{\rho\rho} + \frac{\theta_\rho}{\rho} - \frac{\sin\theta\cos\theta}{\rho^2} - \frac{2\sin^2\theta}{\rho} - h\sin(\theta)\right] + \\ +2\left(\theta_\rho - 1\right) m_\rho = 0, \\ m_{\rho\rho} + \frac{m_\rho}{\rho} + m\left[\theta_\rho^2 + \frac{\sin^2\theta}{\rho^2} - \theta_\rho - \frac{\sin\theta\cos\theta}{\rho}\right] + \\ +2am + 4m^3 - h\cos(\theta) = 0 \qquad (10)$$

with boundary conditions $\theta(0) = \pi$, $\theta(\infty) = 0$, $m(\infty) = m_0$ describe the structure of isolated Skyrmions (the magnetization of the homogeneous phase m_0 is derived from equation $2am + 4m^3 - h = 0$). Typical solutions $\theta(\rho)$, $m(\rho)$ of Eqs. (10) are plotted in Fig. 1.

For present work, we have evaluated numerically the solutions for the energy functionals of type Eq. (1) within a standard approach using finite differences for gradient terms and adjustable grids to accommmodate modulated states with periodic boundary conditions. Search for modulated states and energy minimization was done by Monte Carlo simulated annealing. For 2-dimensional models, this approach can give converged results, as checked by comparison with analytical results. Including secondary effects, the approach is able and has been used by us to calculate thermodynamic stability of phases, and to study the complete temperature-field phase diagrams in terms of equilbrium (mean-field) states of the energy functionals Eq. (1). As we are investigating here long-period modulated phases, the phase diagrams are expected to give qualitatively the correct results for these phenomenological models.

[1] I.E. Dzyaloshinskii, Sov. Phys. JETP **19**, 960.

[2] A. N. Bogdanov et al., Phys. Rev. B **66**, 214410 (2002);

[3] R.M. Hornreich et al., Phys. Rev. Lett. **48**, 1404 (1982).

[4] D. C Wright, N. D. Mermin, Rev. Mod. Phys. **61**, 385 (1989).

[5] A.N. Bogdanov and D.A. Yablonsky, Sov. Phys. JETP **68**, 101 (1989).

[6] A. Bogdanov, A. Hubert, J. Magn. Magn. Mater. **138**, 255 (1994); *ibid.* **195**, 182 (1999); A. Bogdanov, JETP Lett. **62**, 247 (1995); A.N. Bogdanov et al., Physica B **359**, 1162 (2005).

[7] U.K. Rößler et al., Nature **442**, 797 (2006).

[8] X. Z. Yu et al., Nature **465**, 901 (2010).

[9] A. N. Bogdanov, U. K. Rößler, Phys. Rev. Lett. **87**, 037203 (2001).

[10] M. Bode et al., Nature **447** 190 (2007).

[11] U. Tkalec et al., Phys. Rev. Lett. **103**, 127801 (2009).

[12] P.G. de Gennes, in *Fluctuations, Instabilities, and Phase transitions*, ed. T. Riste, NATO ASI Ser. B, vol. 2 (Plenum, New York, 1975).

[13] P. Bak and M. H. Jensen, J. Phys.C: Solid State Phys. **13**, L881 (1980); O. Nakanishi et al., Solid State Comm. **35**, 995 (1980).

[14] J. W. Felix et al., Phys. Rev. Lett. **57**, 2180 (1986).

[15] I. Sosnowska et al., J. Phys. C **15**, 4835 (1982); A. Zheludev et al. Phys. Rev. Lett. **78**, 4857 (1997).

[16] B. Schaub, D. Mukamel, Phys. Rev. B **32**, 6385 (1985).

[17] C. I. Gregory et al., J. Magn. Magn. Mater. **104-107**, 689 (1992); D. Lamago et al., Physica B **385-386**, 385 (2006).

[18] B. Lebech et al., J. Magn. Magn. Mater. **140**, 119 (1995).

[19] S. Muhlbauer et al., Science, **323**, 915 (2009).

[20] C. Pfleiderer et al., Nature **427**, 227 (2004).

[21] C. Pappas et al., Phys. Rev. Lett. **102**, 197202 (2009).

[22] T. H. R. Skyrme, Proc. Roy. Soc. Lon. **260**, 127 (1961).

[23] I. E. Dzyaloshinskii, Sov. Phys. JETP **5**, 1259 (1957), T. Moriya, Phys. Rev. **120**, 91 (1960).

[24] P. G. De Gennes and J. Prost, *The Physics of Liquid Crystals* (Oxford University Press, Oxford, 1993), 2nd ed., D. C Wright, N. D. Mermin, Rev. Mod. Phys. **61**, 385 (1989).

[25] E. H. Brandt, Rep. Prog. Phys. **58**, 1465 (1995), Phys. Rev. B, **68**, 054506 (2003).

[26] See, e.g., J.-C. Tolédano, P. Tolédano, *The Landau Theory of Phase Transitions*, World Scientific, Singapore 1987, chap. V and chap. VI,6.

[27] Yu. A. Izyumov, Sov. Phys. Usp. **27**, 845 (1984).

[28] G. G. Lonzarich, L. Taillefer, J. Phys. C. **18**, 4339 (1985), M. Yamada et al. J. Alloys Comp. **364**, 37, (2004).

[29] M. L. Plumer, M. B. Walker, J. Phys. C. **14**, 4689 (1981), M. L. Plumer, J. Phys.:Cond Matt. **2**, 7503 (1990).